Galvanic Corrosion and Mechanical Behavior of Fiber Metal Laminates of Metallic Glass and Carbon Fiber Composites

Lee Hamill[1,*], Douglas C. Hofmann[2] Steven Nutt[1]

1. Department of Chemical Engineering and Materials Science, University of Southern California, Los Angeles, CA 90089, USA

2. Jet Propulsion Laboratory, California Institute of Technology, Pasadena, CA 91101, USA

Abstract:

The possibility of galvanic corrosion typically prohibits the pairing of carbon fiber and aluminum in a fiber metal laminate (FML). In this study, we describe a new type of FML comprised of alternating layers of bulk metallic glass (BMG) and carbon fiber reinforced polymer (CFRP) composite. We compare the galvanic coupling and mechanical behavior of an Al-based FML and a BMG-CFRP FML. Results showed that when paired with CFRPs, BMG exhibits far less galvanic corrosion than aluminum paired with CFRP. In fact, the corrosion between BMG and CFRP was similar in magnitude to the corrosion between aluminum and glass fiber, the two constituent materials of GLARE, the most widely used FML. While interlaminar shear strength and flexural strength were similar for both FML types, the tensile strength and modulus of BMG-based FMLs were greater than those of Al-based FMLs.

Key words: carbon fiber, fiber metal laminates, corrosion, metallic glass, mechanical properties

1. Introduction

The development of fiber metal laminates (FMLs) began at Delft University in the 1970s as part of an effort to develop high-strength, low-density materials to replace monolithic aluminum for certain aircraft parts. [1] FMLs are laminate structures that consist of alternating layers of metal and composite and are designed to achieve certain properties that exceed those of either constituent individually. The first rendition, ARALL, consisted of aluminum as the metal layer and aramid fiber reinforced epoxy as the composite layer. ARALL was succeeded by GLARE, in which the aramid fibers were replaced with glass fibers, a stronger, less costly material that was more versatile. [2]

In addition to high strength and low density, GLARE exhibited fatigue resistance superior to monolithic aluminum - cracks initiating in the aluminum surface layers arrested upon reaching the composite layer, greatly reducing the risk of fatigue failure. Fatigue resistance is a primary design driver for airframes and skins, as the pressurization and depressurization cycles imposed for each flight introduce a cyclic loading pattern, and stochastic cyclic loading arises from air turbulence and vibrations. The well-known Aloha Air accident, in which the top of the fuselage ruptured during flight, was attributed to high-cycle fatigue, and led aircraft manufacturers to seek materials with greater fatigue resistance. [1, 3] Airbus incorporated GLARE into aircraft design - over half of the fuselage of the A380 consists of GLARE. [4] In addition to meeting desired properties such as high strength, high elastic modulus, improved toughness, corrosion resistance, and fatigue, the shift resulted in a 30% weight reduction. [1, 3, 5, 6]

Currently, the design of Al-based FMLs is restricted to the use of fiberglass, as the risk of galvanic corrosion prohibits the use of carbon fiber reinforced polymer (CFRP) composites. Thus, designers are unable to leverage the superior specific modulus and strength of CFRPs, limiting the property space available to designers. [1–3, 6–11] Galvanic corrosion occurs when two dissimilar conductive materials are exposed and electrically connected by an electrolyte. In FMLs, the polymer matrix of the CFRP in principle electrically isolates the two conductive materials; however, the two components are exposed at free edges of the laminate and can be electrically connected in the presence of an electrolyte.

Previous research has explored galvanic corrosion between fiber composites and various metals. Tavakkolizadeh et. al reported that galvanic corrosion occurred when carbon fibers were in electrical contact with steel in an electrolyte, and they showed that by coating the carbon fibers with epoxy, the rate of galvanic corrosion was reduced, although not eliminated.[12] Ireland et. al considered the effect of including carbon nanotubes in glass fiber (GF) reinforced epoxy composites on galvanic corrosion with aluminum. They reported that galvanic corrosion occurred for the composites modified with carbon nanotubes, despite the polymer barrier between the two conductive materials. [13] Other studies demonstrated that certain metals (titanium, anodized aluminum, and certain stainless steel alloys) resulted in various degrees of galvanic corrosion when paired with CFRPs. [14, 15]

In this study, the pairing of bulk metallic glass (BMG) with carbon fiber reinforced polymer (CFRP) composite in a FML structure was explored. BMGs are distinguished by a non-crystalline microstructure and high strength and elastic limit. [16, 17] Although metallic glasses are well-known commercial products, they have normally been used in thin magnetic ribbons for

use in the transformer industry or as large castings for electronic devices and golf clubs (thus called bulk metallic glass). Until recently, tough and corrosion-resistant BMGs have never been manufactured in a form factor suitable for the use in laminates, which would normally be in the range of 50-200 μm thick sheetmetal. In the current study, a tough Zr-based BMG was manufactured into a continuous roll of sheetmetal 150 μm thick, allowing for the first experimentation on a BMG material that has the potential to be scaled up into mass production.

BMGs also exhibit high corrosion resistance, due to the formation of passive oxide layers and the absence of grain boundaries, and thus are suitable candidates for CFRP-based FMLs. Previous studies identified factors that contribute to the corrosion resistance of BMGs. Peter et al. investigated the corrosion behavior of Zr-based BMGs relative to crystalline counterparts and discovered that while there was no statistically significant difference between corrosion potentials for each, the difference in pitting potential and protection potential indicated that crystalline metal is less immune to pitting corrosion than non-crystalline metal. [18] Pitting corrosion occurs preferentially at grain boundaries, so the absence of grain boundaries increases a metal's resistance to corrosion. Other studies have cited the strong passive oxide layer that forms on BMGs as a factor in their corrosion resistance. [16, 19, 20] Scully et al. specifically cites Zr-based BMGs as having the best anodic passivation ability. [20]

To date, only one study has investigated BMG-CFRP FMLs. Sun et al. evaluated the mechanical performance of FMLs consisting of 30 μm thick Al-Ni-La metallic glass ribbons and unidirectional CFRP. [21] The present study expands on Sun's work by comparing BMG-based and Al-based FMLs with a metal ply thickness that more closely matches those of commercial GLARE (0.2 – 0.5 mm). [22] Analysis includes comparison of galvanic corrosion behavior and

determination of mechanical properties that have been investigated in previous studies of FMLs: interlaminar adhesion [11, 23, 24], bending [25, 26], and tensile [23, 25–30] properties. The results presented in the following sections show negligible galvanic corrosion between BMG and carbon fiber and increased tensile strength and modulus for BMG-based FMLs relative to Al-based FMLs, demonstrating a pathway to higher performance FMLs that incorporate CFRPs.

2. Experimental Procedures

2.1 Materials and FML Fabrication

FMLs were fabricated using two metallic alloys: 2024-F aluminum and a bulk metallic glass ($Zr_{65}Cu_{17.5}Ni_{10}Al_{7.5}$), each with a thickness of 150 μm. CFRP was used for the composite layer, consisting of a toughened epoxy (5320-1, Solvay, Inc.) and unidirectional (HexTow IM7, Hexcel Corporation) carbon fiber tape. Each FML employed the same general stacking sequence; a four-ply, [0/90]s composite layer was placed between each pair of metal layers. Previous research by the authors investigated adhesion methods for BMG-based and Al-based FMLs and determined that the strongest bond was achieved when the metal was initially degreased and an adhesive layer (3M Scotch-Weld Structural Adhesive Film AF 163-2) was included at each composite-metal interface. [31] In this study, metal strips were cleaned with acetone prior to stacking, and the same adhesive layer was included. The number of metal layers, and thus the overall stacking sequence and thickness, varied for each test and is outlined in subsequent sections. Individual samples were cut to size with a diamond blade and precision cutter (Buehler Isomet 4000).

Samples were cured in a vacuum bag assembly in an autoclave, and full vacuum (~95 kPa) was maintained during cure. The cure cycle included a three-hour dwell at 121 °C with a 1.5 °Cmin⁻¹ ramp rate (both up and down). Pressure was applied when the vessel reached 37.8 °C at a rate of 68.9 kPa min⁻¹ to a final pressure of 0.689 MPa which was held for the duration of the temperature dwell.

Sheets of unidirectional dry fibers were used in the galvanic corrosion experiments: carbon fiber (305 g m⁻² Fiber Glast Developments Corp.) and glass fiber (Saertex 955 g m⁻², Fiber Glast Developments Corp.). For one set of corrosion tests, the BMG was devitrified by heating under vacuum to 400 °C (above the glass transition temperature of 375 °C) and holding for 30 minutes. An x-ray diffraction (XRD) pattern was acquired from the devitrified samples to confirm crystallinity (Bruker, D8 Advance).

2.2 Corrosion Testing

Galvanic corrosion between each metal alloy and fiber pair was evaluated by constructing a galvanic cell and monitoring the resulting current. Each galvanic cell consisted of a 2.5 cm² area of the metal and fibers submerged in an electrolyte (3.5% by weight NaCl in DI water), separated by a distance of 2 cm. In this experimental setup, the metal acted as the working electrode, the fibers were connected to ground, and a saturated calomel electrode (SCE) was used as the reference electrode. A galvanostat (VersaStat 3 Potentiostat Galvanostat, Princeton Applied Research) monitored the free-flowing current as a function of time for each galvanic cell.

Long term corrosion was qualitatively monitored. One Al-based and one BMG-based FML were submerged in a salt water bath (3.5% by weight NaCl in DI water) for two weeks. Each FML

followed the stacking sequence outlined in the previous section, contained seven metal layers, and were $16.3 \times 14.2 \times 7$ mm in size. A polished cross-section of each FML was qualitatively evaluated using optical microscopy (Keyence VHX-5000), and an image of each was recorded at 150× magnification prior to submersion. The condition of each sample was re-evaluated after the two-week period.

2.3 Mechanical Testing

Interlaminar, bending, and tensile properties were evaluated using the short beam shear (ASTM D2344), 3-point bend (ASTM D7264), and tensile (ASTM D3039) tests, respectively. All tests were performed on the same mechanical testing device (INSTRON 5567). Approximate dimensions for each type of specimen are given below, with length and width varying by ± 0.5 mm and thickness varying by $\pm 10\%$.

Short beam shear samples contained seven metal layers and were approximately $39.3 \times 13.1 \times 7$ mm. The support span was adjusted for each sample, so that the support span-to-measured thickness ratio was 4.0. Five samples were tested for each FML type, and tests were performed in compression mode at rate of crosshead movement of 1.0 mm min^{-1}. According to the ASTM standard, interlaminar shear strength was calculated using Eqn. 1, where ILSS is the interlaminar shear strength [MPa], P_m is the maximum load [N], b is the measured specimen width [mm], and h is the measured specimen thickness [mm].

$$\text{ILSS} = \frac{3P_m}{4bh} \qquad (1)$$

Three-point bend tests were also performed in compression mode at a speed of 1.0 mm min^{-1}. Five samples for each FML type were tested, and each sample had four metal layers and was

approximately 78.8 × 13 × 3 mm. The support span-to-thickness ratio was chosen to be 19:1 to ensure that the length of each sample was at least 20% greater than the support span. Flexural strength was calculated using Eqn. 2, where σ_m is the maximum stress at the outer surface [MPa], P_m is the peak applied force [N], L is the support span [mm], b is the measured width of the beam [mm], and h is the measured thickness of the beam [mm].

$$\sigma_m = \frac{3 P_m L}{2 b h^2} \qquad (2)$$

Tensile tests were performed on eight samples for each FML type at a displacement rate of 2.0 mm min^{-1}, and a clip-on extensometer was used to record strain information (Instron, 2630-100 series). Sample dimensions were approximately 95 × 9.5 × 1.3 mm, each sample containing two metal layers. To reduce the stress concentration at the grips, end tabs were constructed by adhering two layers of the aluminum ribbon to the top and bottom of each end of the sample with the same film adhesive used within the laminate. Grip length was adjusted for each sample to maintain a gage length of 50 mm. Tensile strength was calculated using Eqn. 3, where σ_T is the tensile strength [MPa], P_m is the peak applied force [N], and A is the average cross-sectional area of the sample [mm^2]. For each sample, the cross-sectional area was calculated at three locations within the gage section by multiplying the measured width and thickness at that point; these three values were averaged to obtain an average cross-sectional area for the sample. Tensile modulus of elasticity (E) was calculated using Eqn. 4, where σ_i is the stress at the ith point (GPa), and ε_i is the strain at the ith point. Points 1 and 2 were chosen by selecting strain values closest to 0.001 and 0.003.

$$\sigma_T = \frac{P_m}{A} \qquad (3)$$

$$E = \frac{\sigma_2 - \sigma_1}{\varepsilon_2 - \varepsilon_1} \qquad (4)$$

3. Results and Discussion

3.1 Corrosion Behavior

Results of the galvanic corrosion tests are displayed in Figure 1 and Table 1. In this test, a greater current density indicates a greater rate of corrosion. The galvanic cell of aluminum and carbon fiber (Al/CF) yielded a current density of 1792.6 mA m^{-2}, while the BMG/CF cell yielded a current density was 96.7 mA m^{-2}, (~ 19× less). The current density of the BMG/CF cell is similar to the current density between aluminum and glass fiber (GF) (16.8 mA m^{-2}, ~ a factor of 5 less). Thus, when Zr-based BMG is used with CFRP to produce FMLs, galvanic corrosion potential is expected to be roughly commensurate with GLARE FMLs currently in use.
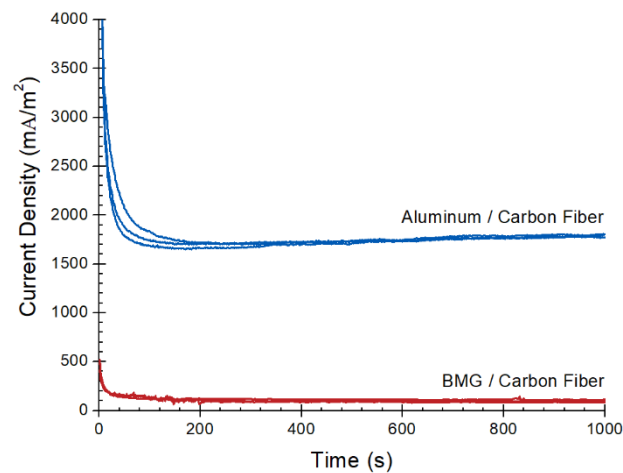

Figure 1: Galvanic corrosion current density exhibited by galvanic cells consisting of aluminum and carbon fiber and BMG and carbon fiber in a saltwater electrolyte solution (3.5% by weight NaCl).

Table 1: Equilibrium current densities for various metal/fiber pairs.

Metal	Fiber	Current Density (mA m^{-2})
Aluminum	Carbon	1792.6
BMG (amorphous)	Carbon	96.7
BMG (crystalline)	Carbon	131.3
Aluminum	Glass	16.8
BMG (amorphous)	Glass	0.2

The long-term corrosion of BMG-based and Al-based FMLs was evaluated by examination of polished sections (Figure 2). Micrographs in Figures 2a and 2b show each FML prior to immersion in the saltwater bath, confirming identical starting conditions. Voids were present primarily within the adhesive layer, and there were few voids within the composite layers or between layers. Fourteen days in the saltwater bath produced vastly different outcomes for each FML (see Figure 2c). As expected from the results of the galvanic corrosion tests, the Al-based FML showed more effects of corrosion than the BMG-based FML. Oxidation of the metal, manifest by a white powdery substance, was clear on all exposed aluminum surfaces, while few blemishes were observed on the BMG-based FML. In fact, the appearance of the BMG-based FML is almost identical to the starting condition, indicating negligible corrosion rate (as expected from Figure 1).

Galvanic corrosion is influenced by multiple factors, including electrode potential, electrolyte chemistry, alloying, heat treatment, surface conditions, and geometry of the materials. Electrode potential of the conductive materials is generally a good predictor for galvanic behavior; faster rates of galvanic corrosion are expected for larger differences in electrode potential of the paired materials. Electrode potentials can vary drastically with electrolyte, so one must also consider the specific material-electrolyte pair of interest. [32] Table 2 gives the electrode potential of relevant elements and alloys in free-flowing saltwater. [33] The aluminum alloy reported here is

Labels within figure a: Aluminum, Adhesive, CFRP, Adhesive, Aluminum, 1 mm

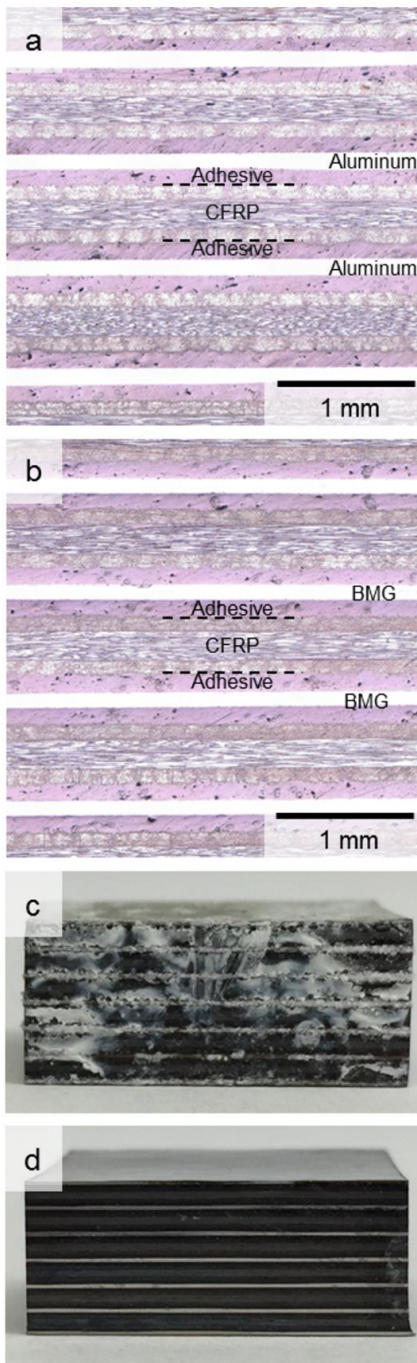Labels within figure b: BMG, Adhesive, CFRP, Adhesive, BMG, 1 mm

Figure 2: *Microscope images of (a) Al-based and (b) BMG-based FMLs prior to submersion in saltwater bath. (c) Al-based and (d) BMG-based FMLs after two weeks in saltwater bath.*

Hamill L, Centea T, Nutt S. Surface Porosity During Vacuum Bag-Only Prepreg Processing: Causes and Mitigation Strategies. Compos Part A Appl Sci Manuf 2015;75:1-10. DOI: doi:10.1016/j.compositesa.2015.04.009

different from the alloy used in this study, and as mentioned previously, alloying can affect

galvanic corrosion behavior. However, there is a large potential difference between the alloy listed

here and graphite (1.04 V), and the electrode potential values for aluminum alloys are known to be

much different from those of carbon and graphite in the galvanic series. The major constituent of

the BMG alloy here was zirconium, with smaller amounts of copper, nickel, and aluminum. The

electrode potential of zirconium is similar to that of graphite (potential difference of 0.29 V).

Nickel and copper have slightly larger potential differences from graphite (0.45 V and 0.61 V,

respectively), although those differences are less than that of aluminum. Because Zr, Cu, and Ni

are all closer to graphite in the galvanic series than aluminum is, alloy composition undoubtedly

contributes to the reduced galvanic corrosion exhibited by the BMG/CF pair.

Table 2: Steady-state electrode potentials of various materials in free-flowing seawater. Potentials are given in reference to a saturated calomel electrode (SCE).[33]

Material	Steady-state electrode potential, V versus SCE
Graphite	+0.25
Zirconium	-0.04
Nickel	-0.20
Copper	-0.36
Aluminum Alloy	-0.79

Microstructure can strongly influence corrosion behavior, since corrosion occurs

preferentially at grain boundaries. [18] The effect of microstructure was investigated by comparing

the corrosion behavior of the devitrified (crystalline) BMG to that of the non-crystalline BMG.

Results were similar to those reported in a previous study by Peter et. al; the corrosion current

density from crystalline BMG was slightly greater than the non-crystalline BMG (Table 1).

However, the current density resulting from the crystalline BMG/CF pair was approximately 14

times less than that of the aluminum/CF pair, indicating that microstructure was a minor factor affecting the corrosion resistance of this BMG.

Surface oxide layers can exhibit different potentials than the base metal, and thus affect corrosion behavior. For example, the standard reversible electrode potential for titanium is negative, but in practice, the electrode potential of titanium in the galvanic series is positive because of the passive oxide layer on the surface. [32] BMGs generally have strong passive oxide layers, and Zr-based BMGs in particular exhibit the greatest passivation capacity. [20] Thus, the passive surface of the BMG undoubtedly contributed to the corrosion resistance observed here.

3.2 Mechanical Behavior

Interlaminar shear strength, flexural strength, and tensile strength of the FMLs are outlined in Table 3. BMG-based FMLs exhibited a slightly greater interlaminar shear strength compared to Al-based FMLs. The failure modes were similar for both FML types - primarily interlaminar shear within the composite layers, as shown in Figures 3a and 3b. Cracks also propagated through the metal layers on occasion (Figures 3c and 3d). Because failure occurred between composite plies (which were identical for both FML types) the values measured for interlaminar shear strength were essentially the same.

Flexural strength values for BMG-based and Al-based FMLs were statistically equivalent, and failure occurred primarily within the composite plies. Typical failure modes included compression of the composite (Figures 4a, 4b, and 4c) and interlaminar shear (Figure 4c). Two of the BMG-based FML samples failed in tension of the outer metal layer (Figure 4d); this failure mode was not witnessed in Al-based FML samples. Although flexural strength was similar for

Table 2: *Steady-state electrode potentials of various materials in free-flowing seawater. Potentials are given in reference to a saturated calomel electrode (SCE).*[33]

	BMG	Al
Interlaminar Shear Strength (MPa)	50.7 ± 1.3 (2.6%)	48.3 ± 0.7 (1.4%)
Flexural Strength (MPa)	808.3 ± 98.3 (12.2%)	827.2 ± 26.4 (3.2%)
Tensile Strength (MPa)	892.9 ± 83.3 (9.3%)	675.6 ± 52.2 (7.7%)
Tensile Modulus of Elasticity (GPa)	50.9 ± 2.6 (5.1%)	45.1 ± 2.3 (5.1%)
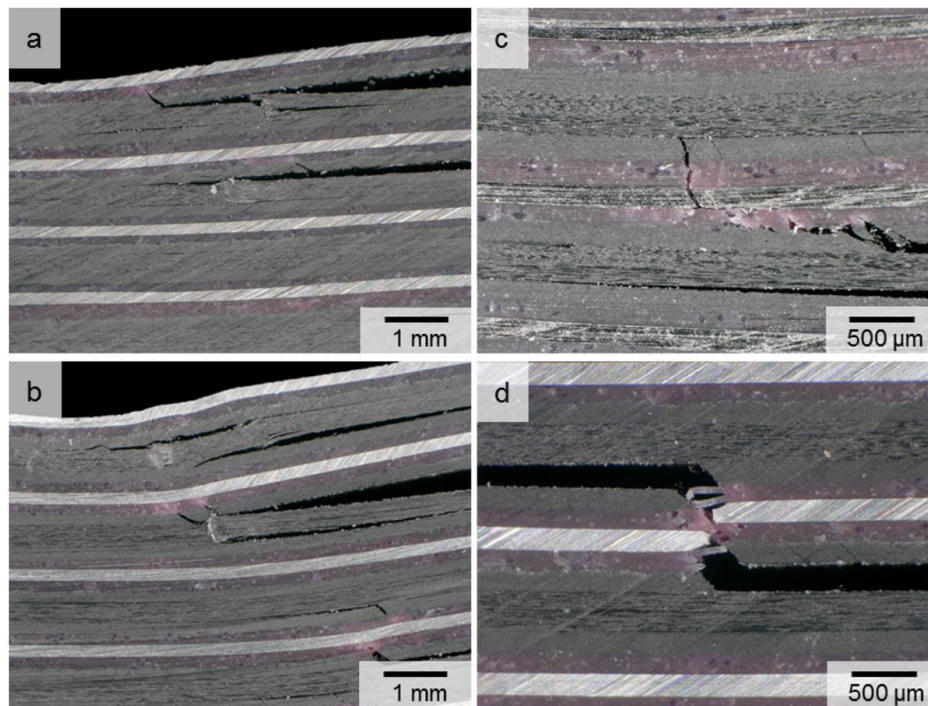
Figure 3: *Microscope images of BMG-based and Al-based FMLs after short beam shear testing. Interlaminar shear of the composite layers (a) and (b), and cracking of the metal shown in (c) and (d) for BMG-based and Al-based FMLs, respectively.*

both FML types, the two FMLs differed in bending stiffness, as manifest in the load-deflection

curves (Figure 5). The slopes of the BMG-based FML curves were greater than those of the Al-

based FML curves, indicating greater bending stiffness. The brittleness observed in the load-

deflection curves is a result of the brittle nature of carbon-fiber composites. Despite this behavior,

composites are widely used as structural materials. Additionally, previous research has shown that there are more ductile alternatives to traditional CFRPs that can be employed in FMLs if desired. [34, 35]
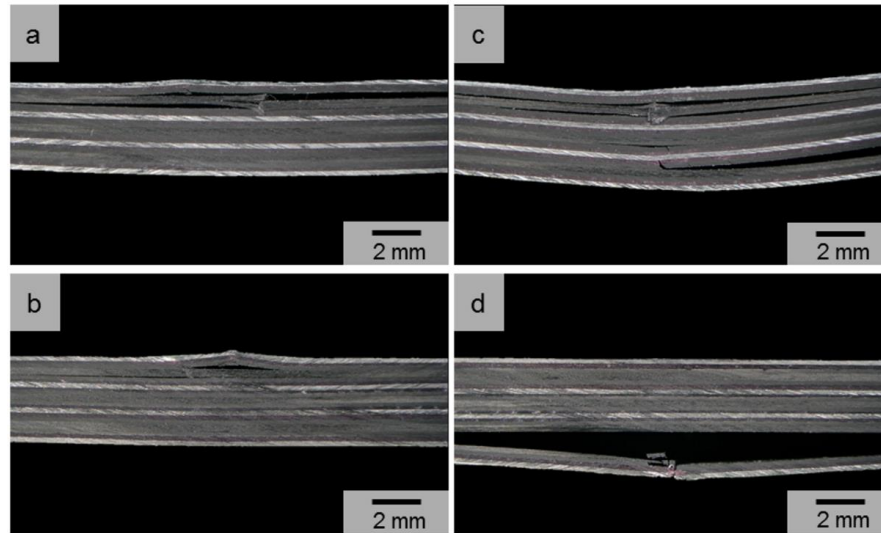

Figure 4: Microscope images of FMLs after 3-point bend testing. Compression failure shown in (a) and (b) for Al-based and BMG-based FMLs, respectively. (c) Multiple failure modes including compression and interlaminar shear in the composite for a Al-based FML. (d) Failure by tension in the outer metal layer for a BMG-based FML.
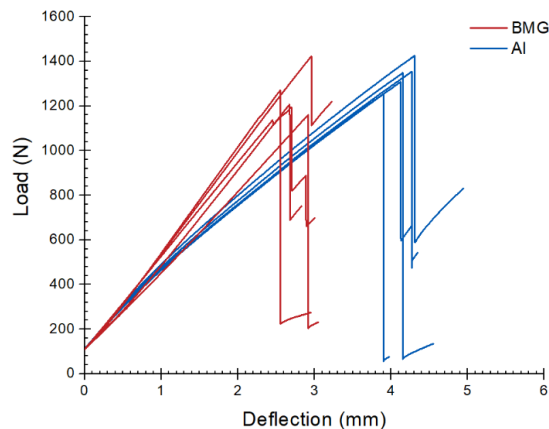

Figure 5: Load-displacement curves for BMG-based and Al-based FMLs during 3-point bend tests.

Hamill L, Centea T, Nutt S. Surface Porosity During Vacuum Bag-Only Prepreg Processing: Causes and Mitigation Strategies. Compos Part A Appl Sci Manuf 2015;75:1-10. DOI: doi:10.1016/j.compositesa.2015.04.009

Average values of tensile strength and modulus of elasticity are reported in Table 3. All eight BMG-based FML samples failed in the gage section, and tensile strength values ranged from 799 – 1072 MPa. Two Al-based FML samples failed in the gage section, while the remaining six failed at the grips. The two samples that failed in the gage section represented the high and low end of the tensile strength range of approximately 614 – 751 MPa. BMG-based FMLs exhibited a greater elastic modulus than aluminum counterparts (50.9 GPa vs. 45.1 GPa for BMG and aluminum, respectively).

As reported by the prepreg manufacturer, the tensile strength and modulus of a $[0/90]_s$ laminate are 1330 MPa and 83.3 GPa, respectively. [36] The reported tensile strength and modulus of Zr-Cu-Ni-Al BMGs range from 1300 – 2000 MPa and 88 – 111 GPa, respectively.[37] The tensile strength of Al 2024-F is roughly an order of magnitude less, ranging from 140 – 210 MPa, and the modulus is reported as 72.4 GPa. [38] Therefore, the BMG-based FMLs are expected to be stronger with greater modulus of elasticity than the Al-based FMLs, and this was confirmed by the results. The BMG-based FML was only about 23% stronger in tension, despite BMG being 500% – 1300% stronger than aluminum. Inspection of the failed samples revealed both CFRP-initiated and metal-initiated failure. CFRP-initiated failure manifested in samples that separated into two pieces, indicating that the CFRP itself failed. Metal-initiated failure was identified in samples that remained in one piece but failed in the metal. Five of the eight BMG-based FMLs exhibited CFRP-initiated failure, while that was the case for only two of the eight Al-based FMLs (of which one failed in the gage section and one failed at the grips).

In CFRP-initiated failure, fibers failed as load increased until only the metal plies remained. Therefore, the tensile strength values for samples with CFRP-initiated failure are

slightly misleading – the metal was the remaining intact component just before failure, which had a smaller cross-sectional area than the FML as a whole. The results indicate that strength is primarily limited by the metal plies in Al-based FMLs and by the composite plies in BMG-based FMLs. In general, BMG-based FMLs were slightly stronger than Al-based FMLs, but similar in elastic modulus, which can be attributed to the CFRP plies.

Figure 6 shows stress-strain curves for a BMG-based and Al-based FML that exhibited metal-dominated failure. A key difference observed in the curves was that the BMG-based FML exhibited purely elastic deformation up until the point of fracture, whereas the Al-based FML exhibited elastic-plastic deformation (as indicated by the change in slope of the stress-strain curve). Yield strengths for Zr-Cu-Ni-Al BMGs are not reported, because they have been shown to undergo only elastic deformation before fracture at a strain of ~1.5%. [39] The individual carbon fibers are reported to fail at an elongation of 1.9%. [40] Al 2024-F, on the other hand, has a reported yield strength of 75 MPa, and a strain to failure of 20%. [38]
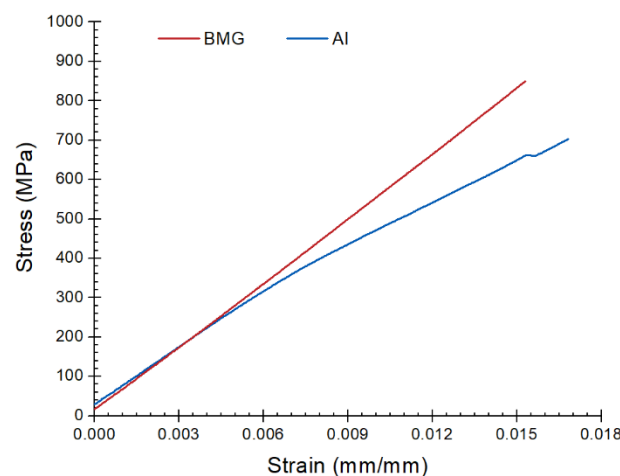

Figure 6: Typical stress-strain curves for a BMG-based and Al-based FML that exhibited metal-initiated failure.

The BMG-based FML reached an ultimate strain of ~1.5% and exhibited metal-initiated failure, indicating that the FML failed because the BMG reached its maximum elongation. The Al-based FMLs began plastically deforming at a stress of approximately 320 MPa and reached an elongation of ~1.7%, demonstrating ductility similar to that of the BMG-based FML. Although Al 2024-F typically undergoes a strain to failure of 20%, [38] the Al-based FML exhibited reduced ductility because of the stress spike that arose in the aluminum sheets. The CFRP-based FML carried a larger stress at a lower strain than monolithic aluminum. As the FML strain increased, fiber failures accumulated within the CFRP, and shed load to the aluminum sheets. The increased load fraction (and stress) caused the stress level in the aluminum plies to reach the tensile strength (140 – 210 MPa), and failure ensued, albeit at a lower strain than normally exhibited by monolithic aluminum.

4. Conclusions

In this study, we demonstrated key characteristic properties of BMG-CFRP FMLs. Mechanical test results revealed that BMG-CFRP FMLs exhibited equal if not superior mechanical properties compared with similar Al-CFRP FMLs. Interlaminar and bending properties were dominated by the composite layers, but tensile strength and modulus values increased when Al plies were replaced with BMG sheets. Compared to traditional GLARE laminates, BMG-CFRP FMLs exhibited superior mechanical performance due to the incorporation of alternative component materials. Particularly notable was the stiffness retention to much higher strains due to the substitution of BMG for aluminum. The retention of elastic behavior to higher strains

(exhibited by BMG-CFRP FMLs) is unusual for metallic structures, and would be potentially useful in applications that require the ability to carry loads but cannot tolerate plastic strains.

Galvanic corrosion results indicated that BMGs were markedly superior to aluminum in terms of corrosion resistance, exhibiting a current density almost 20 times less than that exhibited by aluminum when paired with carbon fiber. In fact, the galvanic corrosion exhibited by BMG-based FMLs is roughly equivalent to that exhibited by GLARE, making it a promising candidate for CFRP-based FMLs.

We have demonstrated that BMG-CFRP FMLs can be produced using Zr-based BMG sheet that is comparable in thickness to the Al sheet metal used in GLARE, and that the combination of mechanical properties are different from and in most cases superior to those of GLARE. The cost of BMGs in general will most likely preclude use in most commercial applications because of the availability of lower-cost materials that meet design specifications. However, BMG alloys exhibit some unique mechanical properties, and as such they may in some cases be uniquely suited to specialized applications. For example, BMG has been identified as a viable option for hypervelocity shielding for spacecraft because of its strength and hardness.[41] Spacecraft shielding is a weight-critical application, motivating the use of composite structures, particularly hard, tough, FMLs. Moreover, the recent development of melt-spinning technologies for creating thick BMG sheetmetal has the potential to sharply reduce the manufacturing cost, presenting a potential pathway to mass production. Pairing BMG sheet stock with CFRP in a FML structure leverages the low density of the CFRP and the high strength and hardness of the BMG. By this approach, BMG-based FMLs can potentially expand the material options that exist for FMLs and provide a pathway to incorporating carbon fiber without risk of corrosion.

References:

[1]   A. Asundi, A.Y.N. Choi, *J. Mater. Process. Technol.* **1997**, *63*, 384.
[2]   C.A.J.R. Vermeeren, *Application of Carbon Fibers in ARALL Laminates - Report LR-658*, **1991**.
[3]   L.B. Vogelesang, A. Vlot, *J. Mater. Process. Technol.* **2000**, *103*, 1.
[4]   B. Kolesnikov, L. Herbeck, A. Fink, *Compos. Struct.* **2008**, *83*, 368.
[5]   T. Sinmazçelik, E. Avcu, M.Ö. Bora, O. Çoban, *Mater. Des.* **2011**, *32*, 3671.
[6]   C.T. Lin, P.W. Kao, F.S. Yang, *Composites* **1991**, *22*, 135.
[7]   C.T. Lin, P.W. Kao, *Compos. Part A* **1996**, *27*, 9.
[8]   G.D. Lawcock, L. Ye, Y.W. Mai, C.T. Sun, *Compos. Sci. Technol.* **1997**, *57*, 1609.
[9]   G. Lawcock, L. Ye, Y.-W. Mai, C.-T. Sun, *Compos. Sci. Technol.* **1997**, *57*, 35.
[10]   Y. Xia, Y. Wang, Y. Zhou, S. Jeelani, *Mater. Lett.* **2007**, *61*, 213.
[11]   E.C. Botelho, L.C. Pardini, M.C. Rezende, *Mater. Sci. Eng. A* **2007**, *452*, 292.
[12]   M. Tavakkolizadeh, H. Saadatmanesh, *J. Compos. Constr.* **2001**, *5*, 200.
[13]   R. Ireland, L. Arronche, V. La Saponara, *Compos. Part B* **2012**, *43*, 183.
[14]   W.C. Tucker, R. Brown, L. Russell, *J. Compos. Mater.* **1990**, *24*, 92.
[15]   F. Bellucci, *Corrosion* **1992**, *48*, 281.
[16]   W.H. Wang, C. Dong, C.H. Shek, *Mater. Sci. Eng. R* **2004**, *44*, 45.
[17]   M. Telford, *Mater. Today* **2004**, 36.
[18]   W.H. Peter, R.A. Buchanan, C.T. Liu, P.K. Liaw, M.L. Morrison, J.A. Horton, C.A. Carmichael Jr, J.L. Wright, *Intermetallics* **2002**, *10*, 1157.
[19]   S.J. Pang, T. Zhang, K. Asami, A. Inoue, *Acta Mater.* **2002**, *50*, 489.
[20]   J.R. Scully, A. Gerbert, J.H. Payer, *J. Mater. Res.* **2007**, *22*, 302.

[21]   B.A. Sun, K.P. Cheung, J.T. Fan, J. Lu, W.H. Wang, *J. Mater. Res.* **2010**, *25*, 2287.

[22]   G. Wu, J. Yang, *JOM* **2005**, *57*, 72.

[23]   L. Ye, A. Afaghi-Khatibi, G. Lawcock, Y. Mai, *Compos. Part A* **1998**, *29*, 1525.

[24]   S.Y. Park, W.J. Choi, H.S. Choi, *Compos. Struct.* **2010**, *92*, 18.

[25]   S.M.R. Khalili, R.K. Mittal, S.G. Kalibar, *Mater. Sci. Eng. A* **2005**, *412*, 137.

[26]   J.G. Carrillo, W.J. Cantwell, *Mech. Mater.* **2009**, *41*, 828.

[27]   T.J. de Vries, A. Vlot, F. Hashagen, *Compos. Struct.* **1999**, *46*, 131.

[28]   P. Cortes, W.J. Cantwell, *Compos. Sci. Technol.* **2006**, *66*, 2306.

[29]   E.C. Botelho, R.S. Almeida, L.C. Pardini, M.C. Rezende, *Int. J. Eng. Sci.* **2007**, *45*, 163.

[30]   J.G. Carrillo, W.J. Cantwell, *Compos. Sci. Technol.* **2007**, *67*, 1684.

[31]   L. Hamill, S.R. Nutt, *Compos. Part B Eng.* **n.d.**

[32]   X.G. Zhang, in *Uhlig's Corros. Handb.*, **2011**, 123.

[33]   in *Met. Handbook, Ninth Ed. Vol. 13*, **1987**, 675.

[34]   Y. Abdin, S. V. Lomov, A. Jain, G.H. Van Lenthe, I. Verpoest, *Compos. Part A Appl. Sci. Manuf.* **2014**, *67*, 171.

[35]   Y. Abdin, A. Jain, I. Verpoest, S. V. Lomov, *Compos. Part A Appl. Sci. Manuf.* **2016**, *91*, 472.

[36]   Cytec Industries Inc., **2015**, *324*, 1.

[37]   D. V Louzguine-Luzgin, L. V Louzguina-Luzgina, A.Y. Churyumov, *Metals (Basel).* **2013**, *3*, 1.

[38]   in *ASM Handb.*, **1990**, 62.

[39]   M. Stoica, J. Das, J. Bednarcik, H. Franz, N. Mattern, W.H. Wang, J. Eckert, *J. Appl. Phys.* **2008**, *104*, 1.

[40]   Hexcel Corporation, **2016**, 1.

[41]   L. Hamill, S. Roberts, M. Davidson, W.L. Johnson, S. Nutt, D.C. Hofmann, *Adv. Eng. Mater.* **2014**, *16*, 85.